TABLE III
MEASURED K-BAND S_ϕ DATA—37 GHz (PER FIG. 3)

f - Hz	γ	$S_\phi(1)$ dB
1 to 5	4	-5
5 to 30	0	-33
30 to 10^3	2.4	+3
10^3 to 3 x 10^4	1.65	-19

An approximate algorithm for c deduced from the exact results for integer γ assuming $f_c \gg f_n$ is $0.375e^{0.2\gamma}$. Table II gives expressions for half-integer values of γ in the range (1.5, 4.5). Additional results for (0, 1) require the parameter f_c explicitly in addition to $S_\phi(1)$ and γ. The approximate correction factor c is identified in the last column.

By using Table III for the S_ϕ data of Fig. 3, the computed values of in Fig. 4 were obtained assuming $c = 1$.

APPENDIX B
USE OF $\sigma_y(\tau)$ TO MODEL ERROR RESPONSE OF SECOND-ORDER PHASE-LOCKED LOOP

Inspection of the curves in Fig. 6 indicate that the Cutler–Searle kernel $K'(u) = \sin^4 u$ approximates the error response of a second-order phase-locked loop.

Substitution of $|1 - H(f)|^2$ for $\sin^4 u$ into (6) while noting that $S_y(f) = f^2 S_\phi(f)/\nu_0^2$ and $f_n = (\pi\tau)^{-1}$ yields (2) directly, after accounting for equal contributions from the T_x and R_x phase noise.

ACKNOWLEDGMENT

The realization discussed in Section IV was done under the Air Force Avionics Laboratory Contract F33615-73-C-4036, T. Joyner, Project Engineer. Most of the experimental data were obtained with the collaboration of E. Perdue and L. Serulneck, both from Raytheon, and R. Hazel, presently at MITRE.

REFERENCES

[1] J. J. Stiffler, *Theory of Synchronous Communications*. Englewood Cliffs: Prentice Hall, 1971, ch. 9.
[2] NBS Technical Note 394, "Characterization of frequency stability," Oct. 1970.
[3] NBS Technical Note 632, "Frequency stability specification and measurement: High frequency and microwave signals," Jan. 1973.
[4] R. Blackman and J. Tukey, *The Measurement of Power Spectra*. New York: Dover, 1959.
[5] R. Bough, "Frequency modulation analysis with the Hadamard variance," presented at the Frequency Control Symp., Apr. 1971.
[6] F. Gardner, *Phaselock Techniques*. New York: Wiley, 1966.
[7] M. Hines, J. Collinet, and J. Ondria, "FM noise suppression of an injection phase locked oscillator," *IEEE Trans. Microwave Theory Tech.*, vol. MTT-16, Sept. 1968.
[8] A. Castro and J. Healy, "Transmitter system for mm-wave satellite communication," presented at the IEEE Int. Commun. Conf., 1975.

A Versatile Millimeter-Wave Imaging System

JAMES P. HOLLINGER, JAMES E. KENNEY, AND BALLARD E. TROY, JR.

***Abstract*—A new millimeter-wave imaging system has been assembled at the Naval Research Laboratory and flight-tested using the NASA/Wallops C-54 aircraft. The system incorporates an oscillating mirror and interchangeable radiometer units making it particularly adaptable to variations in its operational frequency, polarization, and angular resolution. Flight tests of the system have been conducted at 90 GHz and simultaneously at 22 and 31 GHz using a dual frequency radiometer. The imaging system and data processing are described and some of the initial flight test results at 90 GHz are presented.**

INTRODUCTION

PASSIVE microwave imagers have proved to be of great value for the remote sensing of the environment. Various imagers at 10, 19, and 37 GHz have been instrumented and flown aboard aircraft for a wide range of environmental investigations. Two electrically scanning microwave radiometers (ESMR) are currently in use aboard satellites; the 19-GHz ESMR on Nimbus 5 and the 37-GHz ESMR on Nimbus 6. Also on Nimbus 6 is the scanning microwave spectrometer (SCAMS), operating at 22.2, 31.4, 52.85, 53.85, and 55.45 GHz, which employs mechanically scanned reflectors. Microwave imagers have been used in meteorology to infer the thickness and water content of clouds and to map the location and distribution of fronts, convective zones, storms, and areas of precipitation. They have been used to delineate the ice–ocean edge; to locate icebergs, polynyas, and leads; to identify and map ice type and coverage; and to detect and quantify marine oil spills. Over land they have provided information on soil moisture and located field and vegetation boundaries, roads, railroads, and commercial, industrial, residential, and open areas. In addition maps of agricultural, geological, and geographical features have been obtained even at night and even through a snow cover.

Manuscript received December 5, 1976; revised May 4, 1976.
The authors are with the Space Science Division, Naval Research Laboratory, Washington, DC 20375.

The breadth of applications and wealth of information provided by microwave radiometry is due to the variation of the emission, absorption, and reflection properties of matter with the observational frequency, polarization, and incidence angle. For this reason a microwave imaging system with some flexibility and variability in the choice of these operational parameters would be particularly useful in remote-sensing investigations.

Consequently, we have constructed and tested, at the Naval Research Laboratory, a relatively inexpensive passive microwave imaging system which is particularly adaptable to changes in its operational frequency, polarization, and angular resolution. The system has been flight-tested aboard the NASA/Wallops C-54 aircraft. Images have been made at 90 GHz with both 2° and 7° angular resolution. We have also obtained images at two frequencies simultaneously using a dual-frequency radiometer at 22 and 31 GHz.

In this paper we present the first results from this imager. The imaging system is described first, then the data processing is discussed and the results of some of the test measurements at 90 GHz are presented.

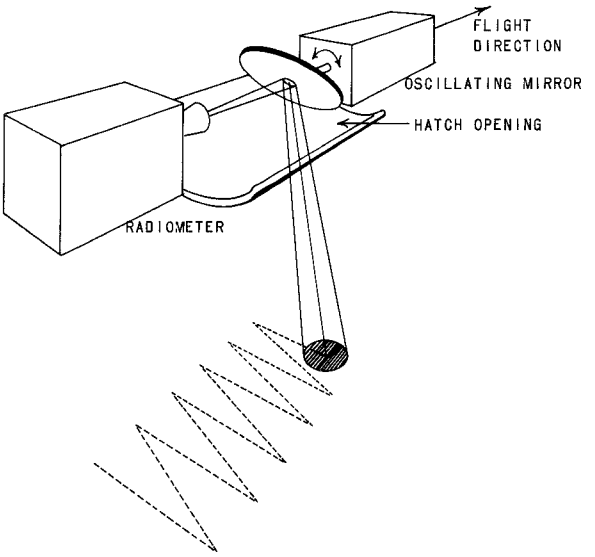

Fig. 1. A sketch of the imager configuration. The oscillating mirror scans the reception pattern of the antenna/radiometer back and forth, forming a zigzag track across the ground with aircraft motion.

System Description

Basically, the imaging system consists of three integral parts: the oscillating mirror, the antenna/radiometer, and the data acquisition unit. Each of these three units is self-contained and may be operated and controlled separately. This design permits different antenna/radiometer combinations to be easily and quickly interchanged. Thus various observational parameters such as frequency, polarization, and beamwidth can be readily varied. In addition it allows a preexisting inventory of radiometers to be used as imagers.

A sketch of the configuration is given in Fig. 1. The antenna/radiometer electrical axis and the rotational axis of the mirror are aligned with the keel of the aircraft. The mirror is scanned at a constant angular rate in a direction perpendicular to the keel, generating a sawtooth or zigzag raster over the ground with aircraft motion. The uniform-rate zigzag scan is preferred over the more easily implemented sinusoidal scan because the time required to scan one resolution cell is constant over the scan width; whereas, the sinusoidal scan moves at a $\pi/2$ greater rate at the center of the scan, where optimum measurement is desired, and more slowly near the edges of the scan. In addition the uniform-rate zigzag scan simplifies data display and processing.

The mirror is elliptically shaped and mounted at an angle of 45° to its rotational axis. Thus the mirror projects the same circular aspect to the antenna at all scan angles. This geometry minimizes output variations with scan angle due to spillover of the antenna power reception pattern past the mirror. The mirror currently being used has a minor axis dimension of 20 cm. This size is adequate for antennas with apertures up to about 15 cm in diameter. It has been used with a 12-cm-aperture horn-lens antenna, a 4.4-cm-aperture corrugated-horn antenna at 90 GHz, and a 15-cm-aperture corrugated horn at both 22 and 31 GHz. Pattern measurements made at 31 GHz with a 13-cm-aperture corrugated-horn antenna show that the pattern reflected from the mirror is identical to the antenna reception pattern, without the mirror down to the sensitivity limit of the measurements of -40 dB, except for one small direct spillover lobe. This lobe is down -31 dB and contains less than 1 percent of the effective solid angle of the antenna. The mirror driver has the capacity to drive larger mirrors which would permit even larger apertures to be used.

The mirror drive was designed and built by John Hill at the Watkins–Johnson Company. The mirror shaft is alternately connected to contrarotating drive shafts by a magnetic clutch to produce the oscillating motion. The contrarotating drives are obtained from a common motor-driven shaft by using gear-to-gear coupling for one sense of rotation and pulley-to-pulley coupling for the opposite sense of rotation. Only the thin magnetic clutch plate, mirror shaft, and mirror reverse direction, minimizing the inertia to be overcome by the drive. Since the drive power required is highest during the very short time when the rotation is reversed, a flywheel is used to store energy during the remainder of the cycle, and only a relatively small electric drive motor is required. The mirror can be scanned at any constant angular rate up to a maximum of 640°/s and it reverses direction in less than 1 ms. The scan width is 64°, resulting in a maximum of 10 scan lines/s.

The polarization of the radiation received by the antenna depends upon the mirror position. Let the polarization of the antenna in the direction of the main beam axis be specified in terms of Stokes parameters [1]:

$$\begin{aligned} I_a &= G_0 \\ Q_a &= G_0 \cos 2\beta \cos 2\chi \\ U_a &= G_0 \cos 2\beta \sin 2\chi \\ V_a &= G_0 \sin 2\beta \end{aligned} \tag{1}$$

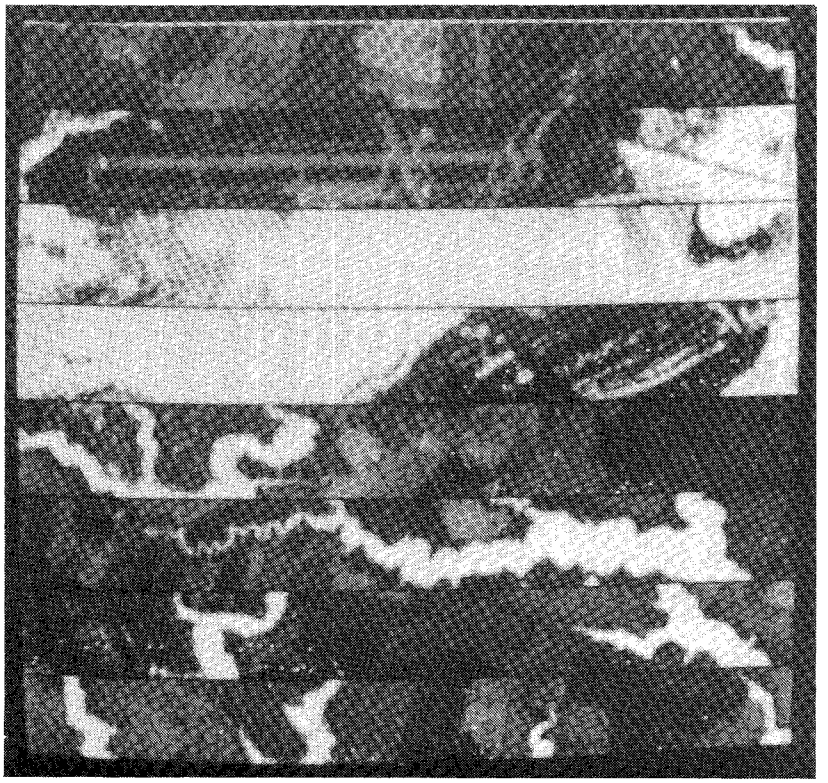

Fig. 2. Unprocessed imagery obtained at 90 GHz. The flight path runs from top left to bottom right along successive rows. White corresponds to low- and black to high-microwave signals.

where G_0 is the on-axis gain of the antenna and $\tan \beta$ is equal to the ratio of the minor and major axes of the polarization ellipse. The position angle χ of the major axis of the ellipse is measured from the vertical in a clockwise direction as viewed from the antenna towards the mirror. The Stokes parameters, after reflection from the mirror and referencing to the plane of incidence on the surface, are given by

$$\begin{aligned} I_s &= G_0 \\ Q_s &= -G_0 \cos 2\beta \cos 2(\theta - \chi) \\ U_s &= -G_0 \cos 2\beta \sin 2(\theta - \chi) \\ V_s &= -G_0 \sin 2\beta \end{aligned} \tag{2}$$

where θ is the position angle of the antenna beam reflected from the mirror measured clockwise from the vertical. The angle of incidence on the surface is then $(\pi - \theta)$, and the position angle of the polarization ellipse measured clockwise from the plane of incidence when viewing the surface is given by $(\pi/2 + \theta - \chi)$. Thus reflection from the mirror rotates the position angle, reverses the sense of polarization from right to left (or vice versa), and leaves the axial ratio unchanged. For example, the measurements presented later in this paper were obtained with a linearly polarized antenna with the electric vector horizontal, and, hence, $\beta = 0$ and $\chi = \pi/2$. The component of the radiation received is then also linearly polarized but with the electric vector oriented at an angle θ to the plane of incidence; thus it lies in the plane of incidence at nadir and varies from vertical polarization for near nadir look angles to an angle of 32° at the scan limits.

The radiometer output is passed through a low-pass filter, sampled at 1° intervals along the scan, digitized with 12-bit precision, and stored in core memory. The sample commands are derived from a shaft encoder driven from the mirror axis, and the low-pass filter is selectable such that the cutoff frequency is less than one-half the sample frequency. Blocks of digitized radiometer data composed of the most recent 128 scan lines along with the housekeeping, aircraft, and radiometer calibration data necessary for processing are recorded periodically on a nine-track magnetic tape. The most recent 100 scan lines are continually displayed in real time on an on-board oscilloscope monitor. A replay mode exists so that 128 line blocks of previously recorded data may be recalled from the magnetic tape and displayed on the monitor.

Data Processing and Test Results

The scene being imaged must be sampled at intervals spaced sufficiently close to preserve the spatial resolution obtainable with the antenna. In the case of reasonably directive antennas, the observed brightness temperature distribution is completely specified by measurements spaced at equal discrete intervals so long as the interval is at least as narrow as one-half the half-power beamwidth of the antenna [2]. Since the surface resolution is generally defined as the projection of the half-power beamwidth on the surface, the scan lines should be spaced at least as close as

one-half the surface resolution and samples should be taken at least at every one-half resolution element along each scan line. Thus the highest surface resolution obtainable is twice the distance the aircraft moves forward in the time required to complete one scan. For an aircraft speed of 60 m/s, about the minimum for the C-54, and a maximum of 10 scan lines/s, the highest resolution obtainable is 12 m and does not depend directly upon the beamwidth. The aircraft altitude for which the highest resolution is obtained does depend upon the beamwidth; larger beamwidths require lower flight altitudes. The resolution achievable in practice depends strongly on the signal-to-noise obtainable with the system. Surface features with a sufficiently high signal-to-noise may be resolved even if they are smaller or more closely spaced than the resolution size given above.

Due to the zigzag character of the scan, the spacing of the scan lines is only uniform in the center of the scan—becoming alternatively too wide and unnecessarily close near the edges of the scan. This can result in aliasing of some spatial frequencies and the generation of Moiré patterns near the scan edges when operating at the highest surface resolution [3]. Although possible, no evidence of this problem has been detected in any of the images obtained to date. For surface resolutions lower than twice the highest resolution, the scan lines are spaced sufficiently close even at the edges of the scan to prevent any aliasing.

In order to facilitate post-flight data editing and analysis, blocks of raw data from the magnetic tape are first displayed on the television monitor of an interactive computer-driven digital image display system[1] [4]. The display screen is composed of 512 by 512 picture elements or "pixels." This allows 32 blocks of 64 samples per scan by 128 scans to be displayed at one time as a series of four blocks per row by eight rows.

A sample of this display is presented in Fig. 2. It contains all the image data obtained during a 7-min portion of a test flight in the vicinity of Wallops Island, Virginia. The flight path runs continuously from left to right along each successive row. The data were obtained at 90 GHz with a 2° half-power beamwidth horn-lens antenna from an altitude of 460 m and at an aircraft speed of 80 m/s. The 90-GHz radiometer has a 1-GHz bandpass and a 0.2 K rms noise output fluctuation for a 1-s integration time constant. This results in a 5 K rms noise output at the sample rate of 640 samples/s and a 2.5 K rms noise per resolution element, since four samples are taken for each resolution element. Here, increasing the microwave signal corresponds to a grey scale running from white to black. Various terrain features may be distinguished such as cultivated fields (darker regions) and wooded areas (darkest regions) in the first row. The bright spot near the end of the first row is a building with a metal roof, which reflects the relatively cold sky. The irregular white region at the end of the first row and beginning of the second row is Little Mosquito Creek. The flight path then passes over the runway at Wallops Station. The white spot on the left end of the runway is a C-54 aircraft. Buildings along the runway appear as lighter regions. Part of the road, causeway, Mosquito Creek, marshland, and Chincoteague Bay follow, with Chincoteague Island and the high school and athletic track appearing just past the middle of the fourth row. The small white dots are tape dropouts. The remainder of the flight path passes over farmland, marshland, and streams of the eastern shore region of Virginia. The entire flight is readily displayed in this manner to provide easy reference to all of the data obtained.

Fig. 3. An example of data processing using a portion of the imagery from the fourth row of Fig. 2. The unprocessed image is at the top; the processed image is shown in the middle. The bottom image shows the result of removing the sharp edges produced by quantizing the image into resolution elements. This improves pattern recognition and ease of viewing without the sacrifice of any significant spatial resolution. The antenna temperature of all three images is given by the grey scale at the bottom.

Those portions of the data selected for detailed analysis are first converted to antenna temperature and then projected into a square grid on the surface. The grid spacing is chosen to be an integral fraction of the scan width in order to preserve commensurability and to be just less than one-half the projection of the half-power beamwidth on the surface in order to preserve all spatial information. A sinc

[1] This image display system was assembled at the Naval Research Laboratory.

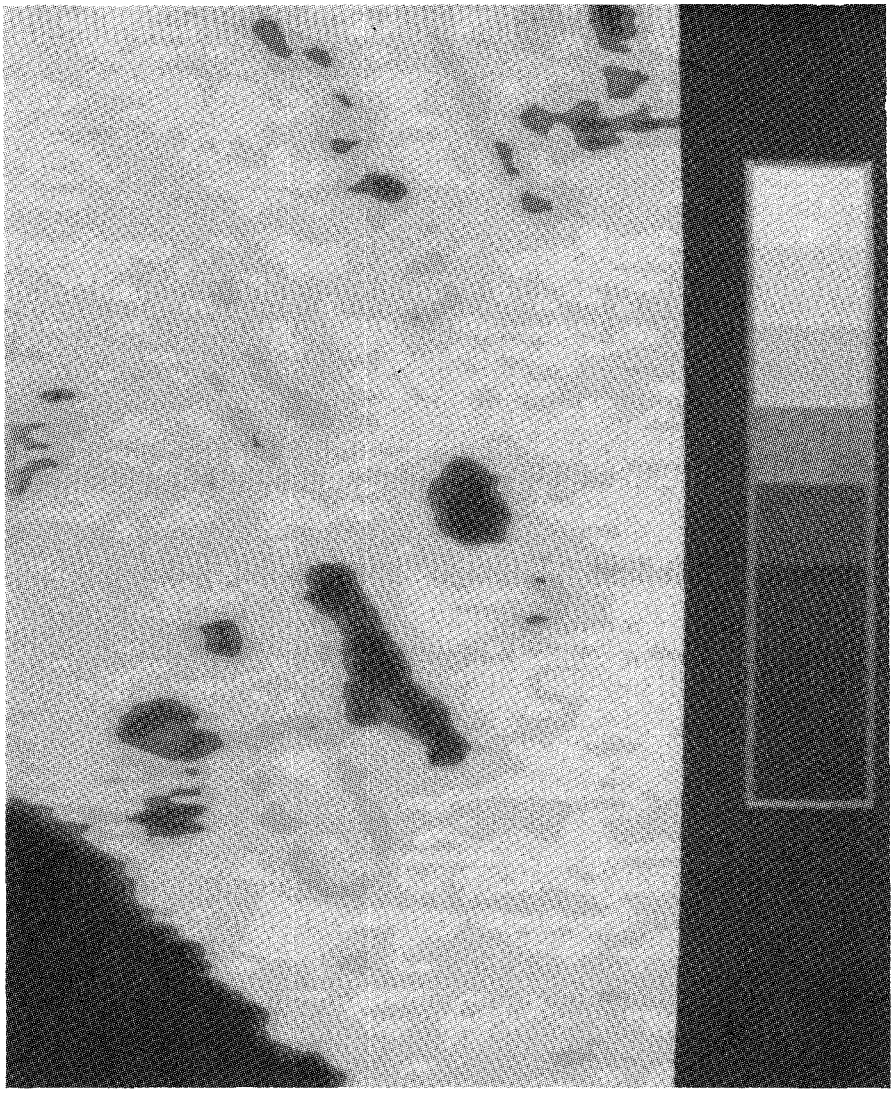

Fig. 4. A contour representation of the image of Fig. 3, obtained by assigning the eight incremental intensity levels shown at the bottom to the antenna temperature. This representation is useful for obtaining coarse quantitative information or for intensity comparison over the image.

function with a spatial cutoff equal to the reciprocal of twice the grid spacing is used to interpolate between the data samples taken at equal-angle intervals along the scan in order to obtain the desired values at the projected grid points [5]. In addition to interpolation, the use of this function filters out all noise and spurious signals at spatial frequencies beyond the surface resolution. The same interpolation-filter sinc function is then applied in the direction orthogonal to the scan direction. The filtering effectively averages the data over a scale size equal to the surface resolution. The aircraft velocity and altitude and the scan rate are taken into account to obtain a square grid and present the true aspect ratio in the image. An example of this processing, using the raw data from block 3, row 4 of Fig. 2; is given in Fig. 3. The unprocessed image is at the top of the figure. The processed image, after projection onto the surface to correct for angular distortion, low-pass filtering to remove all spatial frequencies above the response of the antenna, and adjustment of the aspect ratio to correct for aircraft motion, is shown in the middle of the figure. The image at the bottom of the figure is the processed image after further smoothing, as discussed in the next paragraph, is applied. The intensity of all three images has been converted to absolute antenna temperature and shaded according to the grey scale at the bottom of the figure. Each grid point is represented by a block of four by four pixels and each resolution element by a block of eight by eight pixels on the television monitor.

Processed images from line scanners are often presented in the mosaic form of the middle image of Fig. 3. However, Harmon and Julesz [6] have shown that the visual recognition of portraits which have been coarsely sampled and quantized in this manner is greatly enhanced by blurring the image. Their experiments suggest that the spectral noise generated by sampling and quantizing, which lies adjacent to the picture's spectrum, is most effective in suppressing recognition. The apparent resolution and picture quality as well as the ease with which it may be viewed are strikingly

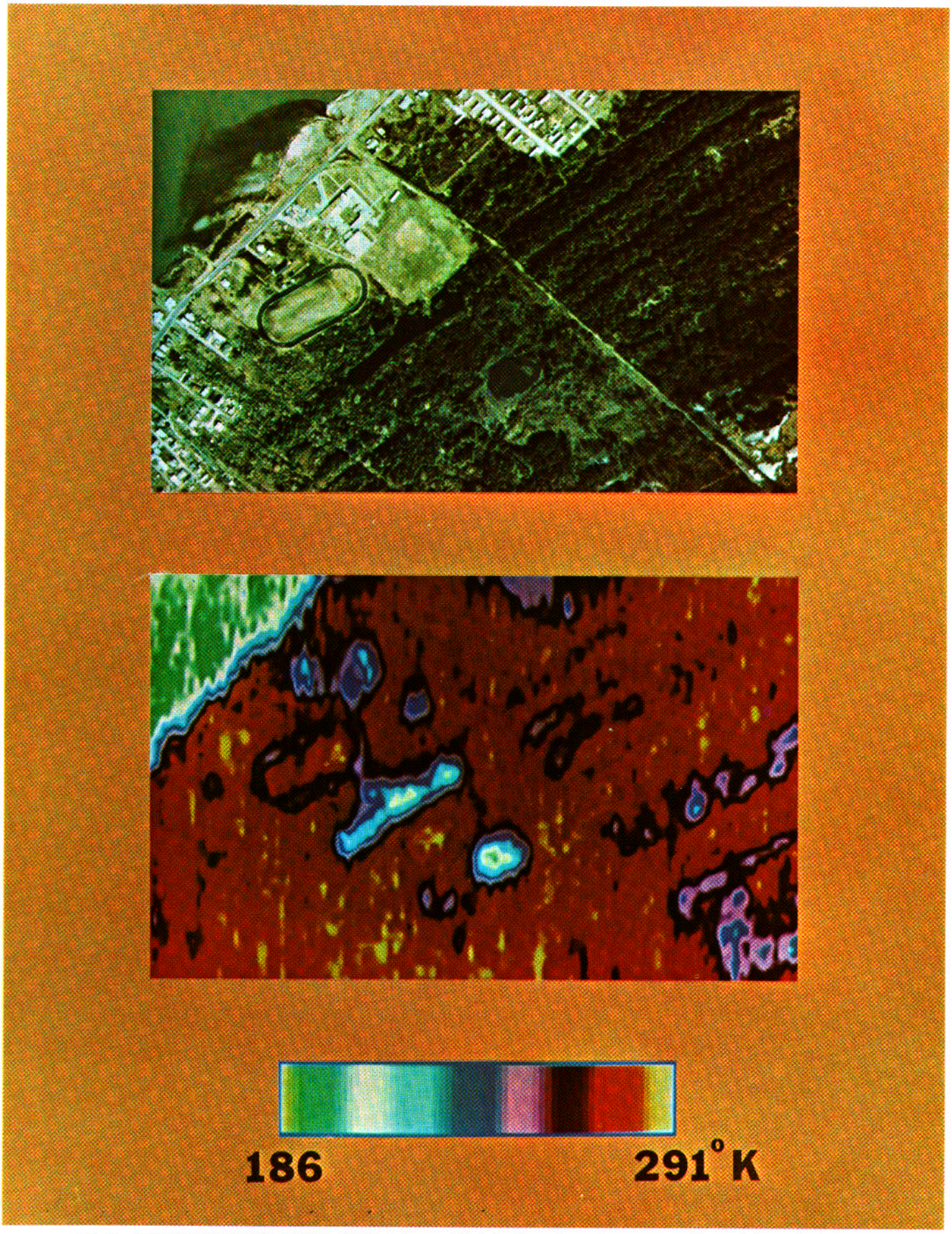

Fig. 5. A 90-GHz image of a portion of Chincoteague, Virginia; the antenna-temperature color scale is at the bottom. An aerial photograph of the same region is at the top. The data were obtained with a 2° half-power beamwidth antenna from an altitude of 460 m and at an aircraft speed of 80 m/s.

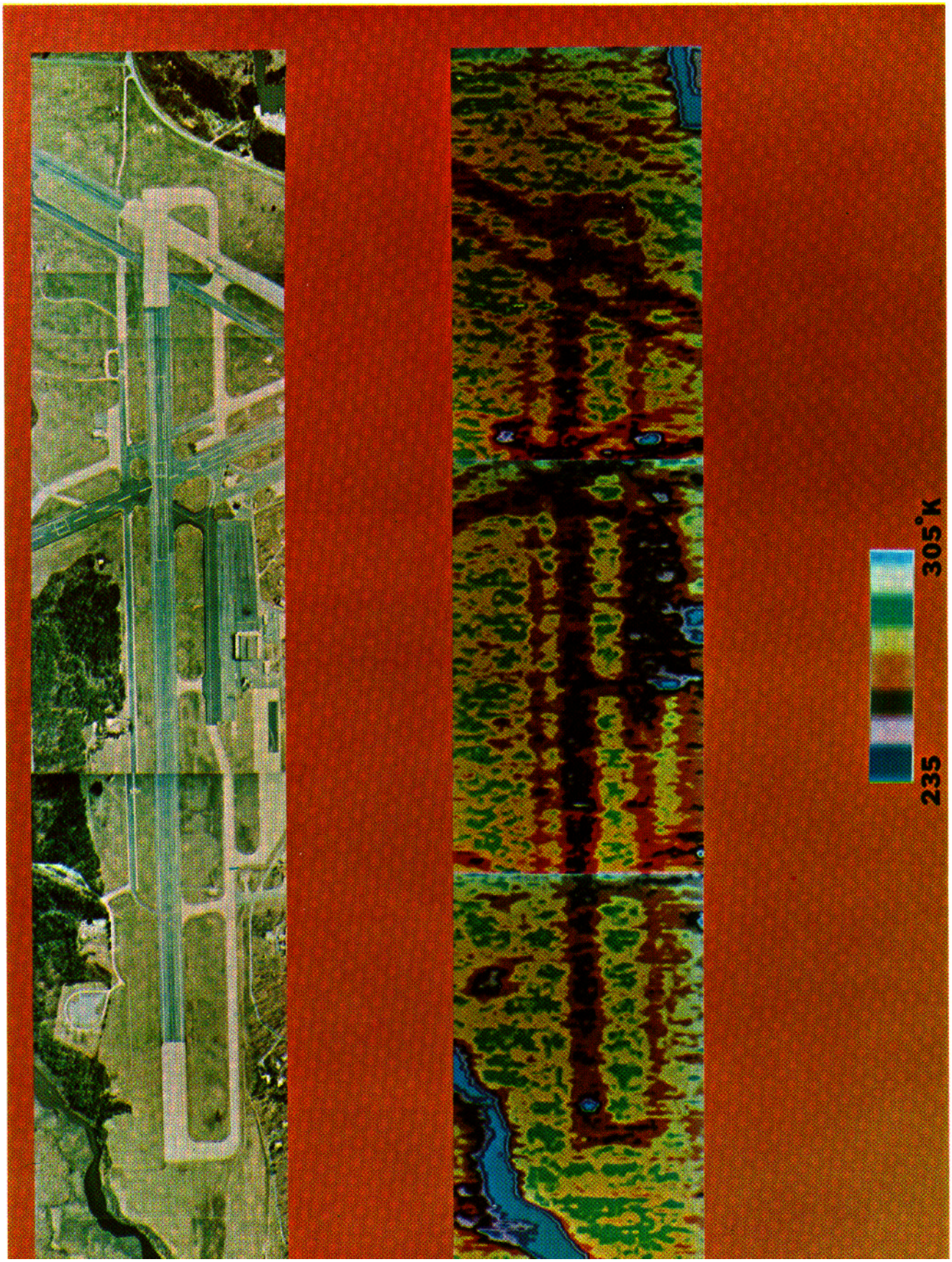

Fig. 6. A 90-GHz image of the runway area at Wallops Station, Virginia, is shown along with an aerial photograph of the region. The antenna temperatures 171–235 K have been compressed in order to enhance the range from 235 to 305 K. The imaged area is 570 by 2900 m.

improved by blurring and smoothing the quantized image. The processed image of Fig. 3 has been further filtered to smooth out the sharp edges of the sample blocks of the image, and is shown at the bottom of Fig. 3. The mosaic or blocky appearance of the image has been removed and it is more relaxing and pleasant to view. The filtering has served only to smooth the hard edges and has not altered any significant spatial frequencies in the image. While we have not made any quantitative study, we feel that this smoothing does enhance the detection and classification of features of the imaged scene and improves the apparent picture quality and ease of viewing. Since the principal purpose of a two-dimensional image presentation is to couple an observer to the measured phenomenon by presenting the measurements in a form most conducive to assimilation and interpretation by him, we have found this smoothing to be of great value.

A useful way of processing the image data when coarse quantitative information is desired is to obtain contours by using an incremental or bar-type grey scale for shading the antenna temperature. A sample of this form of processing is shown in Fig. 4. This is the same image given in the bottom of Fig. 3 but with the antenna-temperature range shaded into eight successive 13 K increments rather than the continuous shading used in Fig. 3.

The use of color allows a finer intensity resolution to be discerned than is possible with black and white presentations since only about 16 shades of grey are identifiable with the eye, whereas 64 different colors may be chosen with our image display system. The image of Figs. 3 and 4 is shown in Fig. 5 with the antenna-temperature scale colored according to the color bar given in the bottom of the figure. An aerial photograph of the imaged area is at the top of the figure. The imaged area is 570 by 970 m. Chincoteague Bay is at the upper left and the large quadrangular building is Chincoteague High School. The track which encloses the athletic field is 9 m wide. In addition to these features, several buildings and various ponds and pools of water may be identified in the microwave image.

A final sample of image data obtained at 90 GHz during the first test flight is shown in Fig. 6. This is the processed and color-coded data from the first three blocks of the second row of Fig. 2. All antenna temperatures below 235 K down to the lowest value present, 171 K, have been assigned the same color given to 235 K in order to enhance the features between 235 and 305 K. The aerial photograph at the top of the figure was taken at a different time from the microwave data, and the C-54 aircraft on the left end of the runway, which appears as a blue region on the microwave image, was not present at the time the photograph was taken. However, lower quality photographs taken simultaneously with the microwave data, using a 35-mm strip-film camera, confirm its presence as well as that of the C-54 aircraft next to the hanger at the bottom center of the image. Various other buildings are distinguishable as cool blue areas along with the streams in the upper left and lower right corners of the image. The network of roads, runways, and taxi strips are identifiable as warmer red–brown colors. Features as small as 6 m are discernible.

Preliminary imaging measurements have also been made at both 22 and 31 GHz simultaneously. A corrugated-horn antenna with an orthogonal dual-mode transducer is used. One output of the transducer is received at 22 GHz and the other at 31 GHz. The outputs from the two radiometers are filtered according to the sampling rate and alternately connected to the input of the data acquisition unit by an analog switch. The switching is performed at each degree along the scan in synchronism with the mirror drive. The result is that the output of one radiometer is sampled and stored at even-degree intervals and the other, at odd-degree intervals. No information is lost so long as beamwidths of 4° or greater are used, and both signals need be sampled no closer than at 2° intervals. The corrugated horn used at 22 and 31 GHz has a beamwidth of 8.4° and 7.9° at the two frequencies, respectively. The two sets of data are later unfolded during computer processing and the two images presented separately.

This same technique can be used to obtain simultaneous images in two orthogonal polarizations at the same frequency. Measurements of the vertical and horizontal linearly polarized radiation and of the left- and right-hand circularly polarized radiation of various targets are planned at 31 GHz. The imaging system will be used at frequencies from 14 to 90 GHz to obtain images of a wide range of both ocean and terrain features at various polarizations and resolutions in the future.

Acknowledgment

We wish to thank J. Hill of the Watkins–Johnson Company for the design and construction of the mirror driver, and H. King, W. Wilson, and T. Mori of the Aerospace Cooperation who designed and built the 90-GHz radiometer. We are indebted to G. Leavitt and K. Hayes of the Engineering Services Division, Naval Research Laboratory, for their design and construction of the data acquisition unit. We are also grateful to J. McGoogan and the pilots, crew, and staff at NASA-Wallops Flight Center for their invaluable assistance and aircraft support for the flight tests.

References

[1] J. D. Kraus, *Radio Astronomy*. New York: McGraw-Hill, 1966, p. 116.
[2] R. N. Bracewell, "Radio astronomy techniques," in *Handbuch der Physik*, vol. 54, 1962, pp. 42–129.
[3] C. D. McGillen and T. E. Riemer, "Moiré patterns and two-dimensional aliasing in line scanner data acquisition systems," *IEEE Trans. Geosci. Electron.*, vol. GE-12, pp. 1–8, Jan. 1974.
[4] I. Jurkevich, J. Lee, and A. F. Petty, private communication.
[5] R. N. Bracewell, *The Fourier Transform and Its Applications*. New York: McGraw-Hill, 1965, p. 62.
[6] L. D. Harmon and B. Julesz, "Masking in visual recognition: Effects of two-dimensional filtered noise," *Science*, vol. 180, pp. 1194–1197, June 15, 1973.